

Analysis of Connection Times in Bipartite Network Data: Development of the Latent Space Accumulator Model with Applications to Assessment Data

Jonghyun Yun¹, Hyunjoo Kim^{2,3}, Minjeong Jeon⁴, and Ick Hoon Jin^{2,3}

¹Institute of Statistical Data Intelligence. USA.

²Department of Applied Statistics, Yonsei University. South Korea.

³Department of Statistics and Data Science, Yonsei University. South Korea.

⁴School of Education and Information Studies, University of California, Los Angeles. USA.

Abstract

Conventional social network analysis typically focuses on analyzing the structure of the connections between pairs of nodes in a sample dataset. However, the process and the consequences of how long it takes pairs of nodes to be connected, i.e., node connection times, on the network structure have been understudied in the literature. In this article, we propose a novel statistical approach, so-called the latent space accumulator model, for modeling connection times and their influence on the structure of connections. We focus on a special type of bipartite network composed of respondents and test items, where connection outcomes are binary and mutually exclusive. To model connection times for each connection outcome, we leverage ideas from the competing risk modeling approach and embed latent spaces into the competing risk models to capture heterogeneous dependence structures of connection times across connection outcome types. The proposed approach is applied and illustrated with two real data examples.

Keywords: Bipartite network; Social network analysis; Connection times; Latent space models; Competing risk models; Assessment data.

1 Introduction

1.1 Background: Bipartite networks

Analyzing bipartite networks have received much attention in a variety of research fields. For example, in sociology, [Agneessens and Roose \(2008\)](#) examined the play choice patterns of theater audiences through bipartite network analysis. [Silk and Fisher \(2017\)](#) proposed bipartite network analysis in animal science to understand the animal social structure and animal behaviors. [Chakraborty et al. \(2019\)](#) applied bipartite network analysis in finance to understand the network structure and its generative process for the Japanese banks and firms. In psychology and education, [Jeon et al. \(2021\)](#) discovered latent interactions between respondents and items in item response data by viewing item response data as a bipartite network. In psychometrics, Recently, [Jeon et al. \(2021\)](#) presented a novel view on assessment data as a bipartite network between respondents and test items in order to alleviate conditional independence and homogeneity assumptions required by traditional item response analysis and to discover unobserved interactions between respondents and test items.

A bipartite network is a network with two disjoint and independent node sets U and V . When a (n, p) bipartite network has n nodes from node-set U and p nodes from node-set V , the network can be represented $n \times p$ rectangular adjacency matrix, $\mathbf{Y}_{n \times p}$. If node k in a node-set U is connected to or associated with node i in a node-set V , then the cell $Y_{ki} = 1$, otherwise 0. A typical approach to analyze a bipartite network is converting a bipartite network into two one-mode networks; if two nodes in node-set U are connected to a node in node-set V , a tie is made between them. However, analyzing two one-mode networks converted from a bipartite network suffers from a loss of information because such analysis ignores interactions between two node-sets U and V .

Several statistical models for directly analyzing bipartite network data have been developed over recent decades. Those include exponential random graph models (ERGM; [Lusher et al., 2013](#)), latent space models (LSM; [Hoff et al., 2002](#); [Handcock et al., 2007](#)), and stochastic block models (SBM; [Lee and Wilkinson, 2019](#)). Features and properties of bipartite network models have been extensively studied in the literature, and various extensions of bipartite network models have been developed.

For example, [Robins and Alexander \(2004\)](#) and [Latapy et al. \(2008\)](#) investigated several network features and network statistics for bipartite networks with extensive simulated and empirical data under certain conditions. [Wang et al. \(2009\)](#) and [Wang et al. \(2013\)](#) proposed new specifications of network statistics for bipartite network analysis with ERGM. [Wang et al. \(2013\)](#) presented a general formulation of a multilevel network structure consisting of a one-mode network that can be defined within a within-

level and a bipartite (two-mode) network can be defined between nodes from two adjacent levels, and extend ERGMs to multilevel networks. [Bomiriya \(2014\)](#) introduced a few network statistics that can be used to measure the homophily effects in a bipartite network with nodal attributes and applied it to ERGM. [Kevork and Kauermann \(2022\)](#) examined the inclusion of specific nodal random effects for first- and second-mode nodes towards an ERGM for bipartite networks in order to account for unobserved heterogeneity in the bipartite network and ensures stable estimation results, especially for large-scale bipartite networks. [Friel et al. \(2016\)](#) analyzed the bipartite temporal network of the leading Irish companies and their directors from 2003 to 2013 with LSM to capture patterns of interaction between directors and companies within a given year and persistence in the interlocking board behavior over time. [Larremore et al. \(2014\)](#) solved the community detection problem for a bipartite network by formulating a bipartite SBM, which explicitly includes vertex type information and may be trivially extended to k-partite networks. [Zhou and Amini \(2019\)](#) considered spectral clustering algorithms for community detection under a general bipartite SBM by proposing a new data-driven regularization that can restore the concentration of the adjacency matrix even for the sparse networks. [Passino and Heard \(2020\)](#) proposed a novel Bayesian model for simultaneous and automatic selection of the appropriate dimension of the latent classes and the number of blocks and extended to directed and bipartite graphs. [Sun \(2021\)](#) constructed a generative bipartite degree-corrected mixed membership SBM and proposed a variational expectation-maximization (EM) algorithm to fit their model.

1.2 Motivation and Proposal

When studying connections between objects in networks, it may be interesting to identify how long it takes the objects to get connected and how the connection times influence the outcomes as well as the structure of the connections. Recently, [Su et al. \(2020\)](#) proposed a latent Cox model to study the relationship between a social network and connection times in the context of analyzing online game users' invitations to friends. To our understanding, [Su et al. \(2020\)](#) is the first and only study that examines the relationship between network connections and connection times, although in this case, the type of connections (i.e., invitation-acceptance) and the type of social network (i.e., friendship) are separate events, and the social network of interest is a one-mode network.

The current paper is motivated by a special type of binary bipartite network composed of respondents and test items obtained from assessment settings. For illustration, let us assume a group of students took an online English vocabulary test. Following [Jeon et al. \(2021\)](#), we can assume that a connection between a respondent and a test item is made when the respondent gives a correct or positive response

to the test item, which creates a bipartite network based on the item response data. In this context, connection time indicates how long it takes a respondent to give a response to a test item, which is typically recorded in log files for computerized assessments. Connection times vary across individuals and test items. Importantly, connection times are likely to show dependence structures. For example, test takers with similar connection times across items may be related to one another compared with those with different connection times. Similarly, test items that show similar connection times across respondents may be more closely related to each other than those items with different connection times. Further, connection times and their dependence structures are likely to depend on the outcomes of the connections. For example, depending on whether the responses are correct or incorrect, which items are closely related or which respondents are closely related can be different.

Focusing on the specialized binary bipartite network based on assessment data, our main interest is to assess the dependence structures induced by connection times between respondents and test items. To this purpose, we propose a Cox model equipped with latent space. Specifically, the proposed model introduces a latent space term to characterize the effects of a hazard function for connection times on the network structures. As aforementioned, a critical feature of the binary bipartite network of our interest is that connections times and their dependence structures largely depend on the outcomes of connections that are mutually exclusive, e.g., correct vs. incorrect or yes vs. no or true vs. false responses. Therefore, by leveraging ideas from competing risk modeling (Fine and Gray, 1999; Lau et al., 2009; Andersen et al., 2012; Ranger and Kuhn, 2014), we propose the hazard functions for connection times to be specific to the two mutually exclusive outcomes of the connections in the proposed model.

The proposed modeling approach is different from [Su et al. \(2020\)](#) in three aspects: First, we work with bipartite networks, whereas [Su et al. \(2020\)](#) works with one-mode networks. Second, connection times and connections are originated from the same process (i.e., respondents responding to test items), unlike [Su et al. \(2020\)](#) where the connection times do not come from the same process (user invitations vs. friendship). Third, we additionally take into account that the outcomes of connections are mutually exclusive and the network structures, e.g., relationships between respondents and items, relationships between respondents, relationships between items, induced by connection times can be heterogeneous depending on the outcomes of the connections. We develop a fully Bayesian approach for estimating the proposed model. We further present an analysis pipeline for the efficient interpretations of associated model parameters and the identification of dependence structures.

The remainder of this article is organized as follows. In Section 2, we describe the proposed model in detail. In Section 3, we present the proposed Bayesian inference method. A simulation-based model

assessment is also established here. In Section 4, we provide two real data applications of the proposed approach using a computer-based Chess game and a mobile language assessment app in Section 4. We close our paper with conclusions in Section 5.

2 Model

2.1 Setup

Suppose $\mathbf{Y}_{n \times p}$ is an undirected bipartite network, whose nodes are divided into two disjoint sets A and B , and each edge represents a connection between a node in A to a node in B . The outcome of y_{ki} represents two types of a connection, e.g., connected vs. disconnected; positively vs. negatively associated between node $k, k = 1, \dots, n$ that belongs to the node-set A and node $i, i = 1, \dots, p$ that belongs to the node-set B . Without loss of generality, we assume $n > p$. We additionally assume y_{ki} is associated with connection-time t_{ki} . In the current context, we focus on assessment scenarios where y_{ki} represents respondent k 's correct vs. incorrect or positive vs. negative responses to test item i , which defines connection vs. disconnection in a bipartite network composed of respondents and test items. In this case, t_{ki} is the observed time that respondent k spent to answer item i , regardless of the outcome of the item response (e.g., correct or incorrect).

2.2 Proposed Model: Latent Space Accumulator Model

Given this special type of bipartite network, our goal is to estimate the dependence structure of pairs of nodes based on their connection times and connection outcomes, and visualize the estimated dependence structure in a two-dimensional latent space, called an interaction map. A notable feature of the described bipartite network of interest is that the outcomes of connections, e.g., correct vs. incorrect responses, are mutually exclusive and the dependence structure of connection times is likely to be heterogeneous across the two types of connection outcomes. Hence, to characterize the heterogeneous dependence structures of connection times between pairs of nodes in a bipartite network, we propose the following Cox model (Cox, 1972; Cheng et al., 1995, 1997; Fine et al., 1998) equipped with Euclidean distances between two nodes in a latent space (Hoff et al., 2002; Handcock et al., 2007; Krivitsky et al., 2009; Raftery et al., 2012; Friel et al., 2016; Jeon et al., 2021) for a hazard function specific to the type of connection outcome:

$$h_{kic}(t) = \lambda_{ic}(t) \exp \left(\theta_{kc} + c \cdot \|\mathbf{z}_k - \mathbf{w}_i\| \right), \quad (1)$$

where $c \in \{-1, 1\}$ represents a connection type, θ_{kc} represents the latent trait of node k for connection type c , $\lambda_{ic}(t)$ represents an unspecified baseline hazard function for node i and connection type c , $\mathbf{z}_k \in \mathbb{R}^d$ and $\mathbf{w}_i \in \mathbb{R}^d$ are embedded latent positions of node k and i in the node-set A and B , respectively, in the d -dimensional Euclidean latent space, and $\|\cdot\|$ represents the Euclidean norm. For the type of connection, $c = 1$ represents a connected dyad (positively or correctly answered), whereas $c = -1$ represents a disconnected dyad (negatively or incorrectly answered). The latent trait of node k , θ_{kc} , constitutes the propensity of node k towards a connection type c on the hazard function.

The baseline hazard function is specific to the connection type and depends on the tendency of the latent trait of node i towards the connection type. We assume a piecewise constant baseline hazard function (Ibrahim et al., 2001), which provides flexible learning of unspecified dependence between connection type and connection times. We place $J + 1$ points $0 = s_0 < s_1 < \dots < s_J < \infty$ that are used for the piecewise exponential approximation of the baseline hazard function:

$$\lambda_{ic}(t) = \lambda_{ic,j} \quad \text{if} \quad s_{j-1} \leq t < s_j, \quad (2)$$

for $j = 1, 2, \dots, J$. This approximation casts the cumulative baseline hazard function as

$$\Lambda_{ic}(t) = (t - s_{j-1})\lambda_{ic,j} + \sum_{m=0}^{j-1} (s_m - s_{m-1})\lambda_{ic,m},$$

for $s_{j-1} \leq t < s_j$. A baseline hazard $\lambda_{ic,j}$ can be interpreted as the propensity of node i towards connection type c on the hazard function in a given time interval $s_{j-1} \leq t < s_j$.

The latent distance in the hazard function aims to account for the heterogeneous interactions between different types of nodes in terms of connection times per connection type. As distance $\|\mathbf{z}_k - \mathbf{w}_i\|$ increases, the hazard function for connection type $c = 1$ increases, which leads to a decrease in connection times. In contrast, a decrease in the hazard function for connection type $c = -1$ leads to an increase in connection times. As a result, a large distance between two nodes in a latent space indicates a large difference in connection times between the two connection types. On the other hand, a short distance between two nodes indicates little difference in connection times between the two connection types. An estimated latent space configuration helps us understand differences in connection times between the connection types across respondents and test items, i.e., the two types of nodes in the network.

An advantage of the proposed Cox model specific to connection types is that it offers more subtle and in-depth insights on the relationship between pairs of nodes in a bipartite network than an ordinary Cox model. This type of Cox model is closely related to the accumulator model presented in the literature

(Vickers, 1970; Van Zandt et al., 2000; Usher and McClelland, 2001; Brown and Heathcote, 2005, 2008; Ranger and Kuhn, 2014), in the sense that two hazard functions correspond to two distinct accumulators that describe the processes of connection between pairs of nodes. The accumulators are assumed to acquire evidence of each connection type over time. The one that accumulates sufficient evidence first drives the corresponding connection outcome to occur, while the other connection outcome remains unobserved due to the mutual exclusiveness. Thus, we refer to our proposed model as the latent space accumulator model for analyzing bipartite networks with connection times.

Since connection outcome types are mutually exclusive, we can write the overall survival function under the competing risk model framework (Fine and Gray, 1999; Lau et al., 2009; Andersen et al., 2012; Ranger and Kuhn, 2014). Then, the overall survival function $S_{ki}(t) = P(T_{ki} > t)$ can be expressed as

$$S_{ki}(t) = \exp \left(- \int_0^t \sum_{c \in \{-1,1\}} h_{kic}(s) ds \right). \quad (3)$$

The joint density of connection outcomes and connection times can be given as

$$f(T_{ki} = t, Y_{ki} = a) = h_{kia}(t) \exp \left\{ - \sum_{c \in \{-1,1\}} \exp \{ \theta_{kc} + c \cdot \|\mathbf{z}_k - \mathbf{w}_i\| \} \Lambda_{ic}(t) \right\}. \quad (4)$$

Let $\Theta = \{\theta_{kc}\}_{1 \leq k \leq n, c \in \{-1,1\}}$ denote a set of parameters for the latent traits of nodes in node-set A and $\Lambda = \{\lambda_{ic,j}\}_{1 \leq i \leq p, 1 \leq j \leq J, c \in \{-1,1\}}$ denotes a set of baseline hazards regarding nodes in node-set B . Denote $\mathbf{Z} = (\mathbf{z}_1, \dots, \mathbf{z}_n)$ and $\mathbf{W} = (\mathbf{w}_1, \dots, \mathbf{w}_p)$ as the configuration of latent embeddings. Conditional on the latent traits and embeddings, we assume y_{ki} and t_{ki} are independent. Then, the likelihood of our latent space accumulator model is given by

$$f(\mathbf{Y}, \mathbf{T} | \Theta, \Lambda, \mathbf{Z}, \mathbf{W}) = \prod_{k=1}^n \prod_{i=1}^p \prod_{j=1}^J \prod_{c \in \{-1,1\}} \left\{ \lambda_{ic,j} \exp \left(\theta_{kc} + c \cdot \|\mathbf{z}_k - \mathbf{w}_i\| \right) \right\}^{\delta_{ki,j} \nu_{kic}} \times \exp \left[-\delta_{ki,j} \left\{ (t_{ki} - s_{j-1}) \lambda_{ic,j} + \sum_{m=0}^{j-1} (s_m - s_{m-1}) \lambda_{ic,m} \right\} \exp \left(\theta_{kc} + c \cdot \|\mathbf{z}_k - \mathbf{w}_i\| \right) \right],$$

where

$$\delta_{ki,j} = \begin{cases} 1 & \text{if } s_{j-1} \leq t_{ki} < s_j, \\ 0 & \text{otherwise,} \end{cases} \quad \text{and} \quad \nu_{kic} = \begin{cases} 1 & \text{if } y_{ki} = c, \\ 0 & \text{otherwise.} \end{cases}$$

2.3 Interpretation

Here we describe the interpretation of the key model parameters and the tools we prepared to present the estimated results effectively.

- $\lambda_{ic,j}$ in a baseline hazard function represents the accumulation rate for connection type c that occurs to particular node i in node-set B in a given time interval (s_{j-1}, s_j) . With the accumulation rate difference between connection-types in a given time interval (s_{j-1}, s_j) for a node i , $\Delta\lambda_{i,j} = \lambda_{i(-1),j} - \lambda_{i(1),j}$, we can identify a connection time difference as well as a more likely connection type for node i within a time interval j . A small $\Delta\lambda_{i,j}$ indicates that node i has similar connection times between both connection types in a time interval j , whereas a large $\Delta\lambda_{i,j}$ indicates that node i has distinct connection times for each connection type in a time interval j , implying that node i has a connection type that is more likely to occur in a time interval j . When $\Delta\lambda_{i,j}$ is positive, node i is more likely for connection type -1 in a time interval j .
- θ_{kc} in a connection type specific hazard function represents the accumulation rate for connection c that occurs to particular node k in node-set A . Similarly to $\lambda_{ic,j}$, we can calculate accumulation rate differences in θ_{kc} between two connection types, $\Delta\hat{\theta}_k = \hat{\theta}_{k(-1)} - \hat{\theta}_{k(1)}$. These differences help us identify which connection outcome type is more likely to occur for node k . A small $|\Delta\theta_k|$ indicates that node k shows similar connection times between the two connection types. On the other hand, a large $|\Delta\theta_k|$ implies node k has distinct connection times between the two connection types, indicating that there is an connection outcome that is more likely to occur for node k in overall time periods.
- An estimated latent space for connection times is referred to as an interaction map in this paper, following [Jeon et al. \(2021\)](#), given that the latent space for a bipartite network based on assessment data represents interactions between respondents and test items.

The interaction map offers additional insights on the accumulation rate between nodes k and i for connection type c . For example, by investigating the latent embedding of \mathbf{Z} and \mathbf{W} , we can identify groups of nodes in node-set A and B that appear close together in the map. The pairwise distances between nodes in node-set A and B show pairs of nodes with higher accumulation rates toward a more likely connection outcome type. In the interaction map, a shorter distance between node k and i implies the accumulation rates between two connection types are similar, indicating negligible differences in the connection times between node k and i . In contrast, a larger distance between node k and i indicates the accumulation rates between the two connection types are not negligible, implying that there is a more likely outcome type for the connection between node k and i .

- We examine the cumulative incidence function (CIF) that quantifies the probability that one event

occurs before time t and before the occurrence of the competing event (Austin et al., 2016). Due to the presence of the competing connection outcome types, the CIF is an attractive analysis tool for the proposed approach as it helps us investigate varying degrees of respondent-item interactions over time. Specifically, the CIF of the connection type c for nodes k and i is defined as:

$$\text{CIF}_{kic}(t) = \Pr(T_{ki} \leq t, Y_{ki} = c).$$

CIF can be thought of as the probability that node k has a specific connection outcome type before time t . The CIFs of nodes in node-set A located closely in an interaction map should be similar across connection type c . When nodes k and i are far apart in an interaction map, a relatively steep-and-tall CIF for $c = 1$ is expected. When nodes k and i are closely located to each other, on the other hand, a relatively gradual-and-short CIF for $c = 1$ is expected.

3 Estimation and Model Fit Assessment

3.1 Bayesian Estimation

We propose a fully Bayesian approach for estimating the latent space accumulator model. Bayesian inference is preferable to maximum likelihood due to the under-identification of the latent embedding. For each k, i, c, j , we assume independent priors as follows:

$$\begin{aligned} \pi(\lambda_{ic,j}) &\sim \text{Gamma}\left(0.5\tilde{\lambda}_{ic,j}, 0.5\right), \quad \pi(\theta_{kc}|\sigma^2) \sim \mathcal{N}(0, \sigma^2), \quad \pi(\sigma^2) \sim \text{Inv-Gamma}(a_\sigma, b_\sigma), \\ \pi(\mathbf{z}_k) &\sim \text{MVN}_d(\mathbf{0}, \gamma^2 \mathbf{I}_d), \quad \pi(\mathbf{w}_i) \sim \text{MVN}_d(\mathbf{0}, \gamma^2 \mathbf{I}_d), \quad \text{and} \quad \pi(\log \gamma) \sim \mathcal{N}(\mu_\gamma, \tau_\gamma^2), \end{aligned}$$

where $\text{Gamma}(a, b)$ denotes the gamma distribution with mean a/b and variance a/b^2 , MVN_d denotes a d -dimensional normal distribution, and \mathbf{I}_d is a $d \times d$ identity matrix. We assign a vague prior for $\lambda_{ic,j}$ by setting $\tilde{\lambda}_j = J / \{s_J(J - j + 0.5)\}$ following from Jin et al. (2014). Other hyperparameters are chosen as $a_\sigma = 0.0001, b_\sigma = 0.0001, \mu_\gamma = 0$, and $\tau_\gamma = 2$.

Based on our experience, the inference of Θ is highly sensitive to the variance parameter of θ_{kc} , σ^2 . Additionally, the configuration of latent embeddings depends on the scale parameter γ of the latent space. To avoid selecting sub-optimal tuning parameters, we introduce a layer of hyper priors, $\pi(\sigma^2)$ and $\pi(\log \gamma)$, to learn optimal values of these parameters from data. We choose hyperparameters such that priors are minimally informative to facilitate flexible Bayesian learning.

The Gibbs sampling is employed to obtain posterior samples from

$$\pi(\Theta, \Lambda, \mathbf{Z}, \mathbf{W}, \gamma, \sigma^2 | \mathbf{Y}, \mathbf{T}) \propto f(\mathbf{Y}, \mathbf{T} | \Theta, \Lambda, \mathbf{Z}, \mathbf{W}) \pi(\Theta | \sigma^2) \pi(\Lambda) \pi(\mathbf{Z} | \gamma) \pi(\mathbf{W} | \gamma) \pi(\sigma^2) \pi(\gamma).$$

The random-walk Metropolis-Hastings (MH) algorithm is used to draw samples from the full conditionals for Θ , \mathbf{Z} , \mathbf{W} , and γ . The posterior samples for Λ and σ^2 are directly sampled from their full conditional distributions.

Let $l = 1, \dots, L$ denotes an index of MCMC sample. One iteration of the MCMC sampler can be described as follows:

1. **Update** $\lambda_{ic,j}$: For each i, c, j , we draw $\lambda_{ic,j}^{(l)}$ from Gamma distribution

$$p(\lambda_{ic,j} | \cdot) \propto \pi(\lambda_{ic,j}) \exp \left[\sum_{k=1}^N (\delta_{ki,j} \nu_{ki,c}) \log \lambda_{ic,j} - \lambda_{ic,j} \sum_{k=1}^N I(T_{ki} > s_{j-1}) \right. \\ \left. \times \left\{ \min(T_{ki}, s_j) - s_{j-1} \right\} \exp \left(\theta_{kc}^{(l-1)} + c \cdot \|\mathbf{z}_k^{(l-1)} - \mathbf{w}_i^{(l-1)}\| \right) \right]$$

2. **Update** θ_{kc} : For each k, c , propose θ_{kc}^* from a symmetric proposal distribution and accept it with probability $\min(1, r_{\theta_{kc}}^*)$ where

$$\log r_{\theta_{kc}}^* = \log \pi(\theta_{kc}^*) - \log \pi(\theta_{kc}^{(l-1)}) + \sum_{i=1}^p (\delta_{ki,j} \nu_{ki,c}) (\theta_{kc}^* - \theta_{kc}^{(l-1)}) \\ - \sum_{i=1}^p \Lambda_{ic}(t_{ki})^{(l)} \exp \left\{ c \cdot \|\mathbf{z}_k^{(l-1)} - \mathbf{w}_i^{(l-1)}\| \right\} \exp \left\{ \theta_{kc}^* - \theta_{kc}^{(l-1)} \right\}.$$

3. **Update** \mathbf{z}_k : For each k , propose \mathbf{z}_k^* from a symmetric proposal distribution and accept it with probability $\min(1, r_{\mathbf{z}_k}^*)$ where

$$\log r_{\mathbf{z}_k}^* = \sum_{i=1}^p \sum_{c=\{-1,1\}} (\delta_{ki,j} \nu_{ki,c}) \left(\|\mathbf{z}_k^* - \mathbf{w}_i^{(l-1)}\| - \|\mathbf{z}_k^{(l-1)} - \mathbf{w}_i^{(l-1)}\| \right) \\ - \sum_{i=1}^p \sum_{c=\{-1,1\}} \Lambda_{ic}(t_{ki})^{(l)} \exp \left\{ \theta_{kc}^{(l)} \right\} \left[\exp \left\{ c \cdot \|\mathbf{z}_k^* - \mathbf{w}_i^{(l-1)}\| \right\} \right. \\ \left. - \exp \left\{ c \cdot \|\mathbf{z}_k^{(l-1)} - \mathbf{w}_i^{(l-1)}\| \right\} \right] + \log \pi(\mathbf{z}_k^*) - \log \pi(\mathbf{z}_k^{(l-1)}).$$

4. **Update** \mathbf{w}_i : For each i , propose \mathbf{w}_i^* from a symmetric proposal distribution and accept it with probability $\min(1, r_{\mathbf{w}_i}^*)$ where

$$\log r_{\mathbf{w}_i}^* = \sum_{k=1}^n \sum_{c=\{-1,1\}} (\delta_{ki,j} \nu_{ki,c}) \left(\|\mathbf{z}_k^{(l)} - \mathbf{w}_i^*\| - \|\mathbf{z}_k^{(l)} - \mathbf{w}_i^{(l-1)}\| \right) \\ - \sum_{i=1}^p \sum_{c=\{-1,1\}} \Lambda_{ic}(t_{ki})^{(l)} \exp \left\{ \theta_{kc}^{(l)} \right\} \left[\exp \left\{ c \cdot \|\mathbf{z}_k^{(l)} - \mathbf{w}_i^*\| \right\} \right. \\ \left. - \exp \left\{ c \cdot \|\mathbf{z}_k^{(l)} - \mathbf{w}_i^{(l-1)}\| \right\} \right] + \log \pi(\mathbf{w}_i^*) - \log \pi(\mathbf{w}_i^{(l-1)}).$$

5. **Update** γ : Propose γ^* from a proposal $g_\gamma(\gamma^{(l-1)} \rightarrow \gamma^*)$ and accept it with probability $\min(1, r_\gamma^*)$

where

$$\begin{aligned}\log r_\gamma^* = & \sum_{k=1}^n \log \text{MVN}_d(\mathbf{z}_k^{(l)} | \mathbf{0}, (\gamma^*)^2 \mathbf{I}_d) - \log \text{MVN}_d(\mathbf{z}_k^{(l)} | \mathbf{0}, (\gamma^{(l-1)})^2 \mathbf{I}_d) \\ & + \sum_{i=1}^p \log \text{MVN}_d(\mathbf{w}_i^{(l)} | \mathbf{0}, (\gamma^*)^2 \mathbf{I}_d) - \log \text{MVN}_d(\mathbf{w}_i^{(l)} | \mathbf{0}, (\gamma^{(l-1)})^2 \mathbf{I}_d) \\ & + \log g_\gamma(\gamma^* \rightarrow \gamma^{(l-1)}) - \log g_\gamma(\gamma^{(l-1)} \rightarrow \gamma^*) + \log \pi(\gamma^*) - \log \pi(\gamma^{(l-1)}),\end{aligned}$$

where $\text{MVN}_d(\cdot | \mu, \Sigma)$ denotes a d -dimensional Gaussian density with mean μ and variance Σ .

6. Update σ^2 : We draw σ^2 from Inv-Gamma $\left(a_\sigma + N, b_\sigma + 0.5 \sum_{c \in \{-1,1\}} \sum_{k=1}^N (\theta_{kc}^{(l)})^2\right)$.

We use (multivariate) Gaussian distributions centered at the current values of the parameters and the latent embeddings as symmetric proposal distributions, with diagonal variance-covariance matrices. For the proposal distribution of γ , $g_\gamma(\cdot \rightarrow \cdot)$, we use a log-normal distribution. Variances of the proposal distributions are tuned to achieve an acceptance ratio close to 0.3. To detect non-convergence of the MCMC algorithm, we use trace plots along with the Gelman-Rubin diagnostic (Gelman and Rubin, 1992). The MCMC algorithm was written in R (R Core Team, 2020) and C++ with Stan math library (Carpenter et al., 2017). The code, along with example data sets, is found in <https://github.com/Jonghyun-Yun/LSA>.

Each connection-type-specific hazard function is invariant to translations, reflections, and rotations of the latent positions of nodes because the hazard function depends on the positions through the distances, and the distances are invariant under the aforementioned transformations. As a consequence, the likelihood function is invariant under these transformations like latent space models of network data (Hoff et al., 2002). Such identifiability issues can be resolved by post-processing the MCMC output with Procrustes matching (Gower, 1975).

3.2 Model Fit Assessment

To assess model fit, we simulated data from the posterior predictive distribution $p(\tilde{\mathbf{Y}}, \tilde{\mathbf{T}} | \mathbf{Y}, \mathbf{T})$, where $\tilde{\mathbf{Y}} = \{\tilde{Y}_{ki}\}$ and $\tilde{\mathbf{T}} = \{\tilde{T}_{ki}\}$ denote the generated connection type and connection times for respondent k and item i . The Cox model with piecewise baseline functions leads to a monotone decreasing survival function, and its analytic inverse exists (Walke, 2010). Thus, we use the probability inverse transformation based on the overall survival function to generate the connection times.

Let $g_{ki,j}$ denote the overall hazard function at j -th segment and is given as follows:

$$g_{ki,j} = \sum_{c \in \{-1,1\}} \lambda_{ic,j} \exp \left\{ \theta_{kc} + c \cdot \|\mathbf{z}_k - \mathbf{w}_i\| \right\}.$$

Then, the inverse transformation of the overall survival function is given as

$$t = s_j + \frac{1}{g_{ki,j}} \left[-\log \left\{ S_{ki}(t) \right\} - \sum_{m=1}^j g_{ki,m} (s_m - s_{m-1}) \right], \quad (5)$$

if the survival function is bounded by cumulative overall hazards

$$\sum_{m=1}^j g_{ki,m} (s_m - s_{m-1}) < -\log \left\{ S_{ki}(t) \right\} \leq \sum_{m=1}^{j+1} g_{ki,m} (s_m - s_{m-1}), \quad (6)$$

for some $j \in \{1, \dots, J-1\}$; otherwise the inverse transformation becomes

$$t = \begin{cases} \log \left\{ S_{ki}(t) \right\} / g_{ki,1}, & \text{if } -\log \left\{ S_{ki}(t) \right\} < g_{ki,1} s_1, \\ s_J, & \text{if } \sum_{m=1}^J g_{ki,m} (s_m - s_{m-1}) < -\log \left\{ S_{ki}(t) \right\}. \end{cases} \quad (7)$$

Given the connection times, \tilde{T}_{ki} , the conditional distribution of the connection type is

$$P(\tilde{Y}_{ki} = c \mid \tilde{T}_{ki} = t) = \frac{h_{kic}(t)}{\sum_{c \in \{-1, 1\}} h_{kic}(t)} \quad (8)$$

for each k and i .

Let L denote the total number of MCMC iterations. Algorithm 1 elaborates how to generate the posterior predictive samples of $\tilde{\mathbf{Y}}$ and $\tilde{\mathbf{T}}$.

Algorithm 1: Generate the Posterior Predictive Samples of $\tilde{\mathbf{Y}}$ and $\tilde{\mathbf{T}}$.

```

for  $l$  in  $1:L$  do
  for  $k$  in  $1:n$  do
    for  $i$  in  $1:p$  do
      1. Draw  $-\log \left\{ S_{ki}(t)^{(l)} \right\} \sim \text{Exponential}(1)$ .
      2. Do the probabilistic inverse transformation. If  $-\log \left\{ S_{ki}(t) \right\}$  is bounded as in (6),
         then use (5) to set  $\tilde{T}_{ki}^{(l)}$ . If no such bounds are found, then we use (7) to set  $\tilde{T}_{ki}^{(l)}$ .
      3. Set  $\tilde{Y}_{ki}^{(l)} = c$  with probability  $P(Y_{ki} = c \mid \tilde{T}_{ki} = \tilde{T}_{ki}^{(l)})$ .
    end
  end
end

```

The posterior predictive p-values, or Bayesian p-values, are used to assess model fit to connection times. The p-values are calculated for each k and i to quantify the discrepancy between simulated and observed connection times as follows:

$$P_{B_{ki}} = \frac{1}{L} \sum_{l=1}^L I(\tilde{T}_{ki}^{(l)} \geq t_{ki}). \quad (9)$$

The p-value that lies outside $[0.05, 0.95]$ is thought to be evidence of model misfit. We use classification performance metrics to assess model fit to connection outcome types. Let

$$p_{kic}^{(l)} \equiv P(Y_{ki} = c | T_{ki} = \tilde{T}_{ki}^{(l)}), \quad (10)$$

which can be served as the prediction probability of $Y_{ki} = c$ connection type based on l -th iteration of MCMC samples. To see if these probabilities are close to the observed truth Y_{ki} , we calculate the log-loss as follows:

$$\text{Log-loss}_i^{(l)} = -\frac{1}{N} \sum_{k=1}^N I(Y_{ki} = c) \log p_{kic}^{(l)}, \quad (11)$$

for each item i and sample l . For an additional metric, we estimate receiver operating characteristic (ROC) curves for each item i and sample l by treating $Y_{ki} = 1$ as the positive outcome. Then, the area under the curve (AUC) is obtained to summarize the overall assessment of our model.

4 Applications

In this section, we apply the proposed latent space accumulator model to two real data examples. Both applications are based on computerized assessments where a group of test-takers responds to a set of test items, where the two connection outcomes are correct and incorrect responses, while connection times indicate how long it took for the test takers to give responses to the test items.

By applying the MCMC algorithm described in Section 3.1, we generated the posterior distributions of the model parameters for each example. Three independent MCMC chains were initiated with random starting values. Each chain consisted of 20,000 iterations, with the first halves were discarded as a burn-in. From the remaining samples, we retrieved every 10-th draw (thinning interval) to construct posterior samples.

4.1 Amsterdam Chess Test

4.1.1 Data and Estimation

The first dataset is obtained from a sub-test of the Amsterdam Chess Test (ACT) designed to measure players' chess playing proficiency (van der Mass and Wagenmakers, 2005). The dataset consists of 40 items divided into three sets based on required chess skills: 20 tactical items, 10 positional items, and 10 endgame items with increasing difficulty in each set. Tactical items measure a player's ability of calculating a sequence of moves to gain tangible results, whereas positional items measure how

proficient a player is at improving one's own position by obtaining a superior position while decreasing the opponent's tactical potential. The endgame items mainly measure a player's skills necessary in situations where few pieces are left. Players were asked to find an optimal move for each item within a 30 second time limit. The information of response accuracy and response time were recorded per item for each player.

It is straightforward to translate the ACT data into our modeling framework. Players and items serve as two distinct sets of nodes that build a bipartite network. A player is connected to an item when s/he answered the item correctly, and the response time serves as the connection time between the player and the item. Two connection outcome types are incorrect ($c = -1$) and correct ($c = 1$) answers.

4.1.2 Analysis Results

Accumulation Rate Differences $\Delta\lambda_{i,j}$ The posterior distributions of $\Delta\lambda_{i,j} = \lambda_{i(-1),j} - \lambda_{i(1),j}$ across the 40 test items are presented in Figure 1. The values of $\Delta\lambda_{i,j}$ represent accumulation rate differences in the baseline hazard functions between incorrect and correct connection outcomes for each time interval. Response times were divided into five sub-intervals using the sample quantiles as cut-off points: 1 to 4 seconds for the first interval; 4 to 8 seconds for the second interval; 8 to 13 seconds for the third interval; 13 to 20 seconds for the fourth interval; and 20 to 30 seconds for the fifth interval.

We first grouped the items based on their average response accuracy and response times as follows: (1) group 1: items with high response accuracy and short response time, (2) group 2: items with low response accuracy and long response time, and (3) group 3: items with varying response times across respondents. In group 1, the values of $\Delta\lambda_{i,j}$ tend to be negative, meaning that the accumulation rate is higher toward the correct response outcome. In group 2, $\Delta\lambda_{i,j}$ values tend to be positive, meaning that the accumulation rate is lower toward the correct response outcome. In group 3, we observed $\Delta\lambda_{i,j} \approx 0$, meaning that the accumulation rates are similar for the correct and incorrect response outcomes.

As described in Section 2.3, the analysis of $\Delta\lambda_{i,j}$ across time interval j reveals the individual item's distribution of response accuracy and times. For example, items 1-3 show negative mean values of $\Delta\lambda_{i,j}$ in earlier time intervals. These are fairly easy items where roughly 75% of respondents answered them correctly before $t = 8$ seconds. On the other hand, items 37-39 show $\Delta\lambda_{i,j} \approx 0$ in earlier time intervals (near $t = 1$), while the distributions are shifted upwards to the end of time intervals. These are difficult items with low accuracy (10 – 30%), and response times are evenly distributed over the five-time intervals.

Interaction Map Figure 2a is the estimated interaction maps. In each sub-figure, dots represent respondents (node-set A), and numbers represent items (node-set B). A large distance between a respondent and an item indicates that the respondent-item connection took a short time and high response accuracy. On the other hand, a short distance indicates that the respondent-item connection took a relatively long time and low response accuracy. For example, items 1-5 and items 31-33 are far away from the majority of respondents. This means that these items are generally easy items (i.e., high accuracy) with generally short response times.

To better interpret the interaction map, we grouped the individual respondents with those items that they are meaningfully close to. To this purpose, we applied spectral co-clustering (Dhillon, 2001) based on a radial basis function of $\|\mathbf{z}_k - \mathbf{w}_i\|$. We determined that $K = 3$ was the optimal number of clusters based on the elbow method. The co-clustering result is presented in Figure 2b, with cluster membership represented in red, green, and blue colors. In general, respondents are expected to take a long response time with low accuracy to the items in their cluster membership.

Further, we calculated the accumulation rates difference in θ_{kc} , $\Delta\hat{\theta}_k = \hat{\theta}_{k(-1)} - \hat{\theta}_{k(1)}$, where $\hat{\theta}_{kc}$ denotes the posterior mean of θ_{kc} . We overlaid respondents with $\Delta\hat{\theta}_k$ based on a continuous, colored scale in Figure 2c. As the red color gets darker, $\Delta\hat{\theta}_k$ gets closer to 0, implying there is little response time difference between the two connection types. As discussed in Section 2.3, $\Delta\hat{\theta}_k$ helps identify a connection outcome type that is more likely to occur for respondent k , and we observed the difference is negatively correlated with the respondent's overall response accuracy.

We found that respondents near the boundaries of the space between red and green clusters tend to have small values of $\Delta\hat{\theta}_k$, indicating high accumulation rates toward correct responses in general. On the contrary, in the blue cluster and the top of the red cluster, respondents tend to show lighter red dots, suggesting that they have high accumulation rates toward incorrect responses in general.

By closely inspecting item-respondent distances in Figure 2c, we identified item-respondent pairs with a high propensity for connection type $c = 1$ (i.e., tendency of correctness). For example, respondents at the bottom of the green cluster are far away from items 35, 37, and 38, meaning they were more likely to solve these items correctly within a fairly short response time. On the other hand, these respondents were close to items 18 and 28, meaning that they were more likely to solve these items incorrectly with a long response time. Note that all these five items (items 18, 28, 35, 37, and 38) have low accuracy rates (around 10 - 40%). The results discussed above suggest that our approach can differentiate subtle individual differences in the correctness of responses as well as the length of response times.

Lastly, we overlaid individual respondents with their ELO ratings, an external measure representing

a chess player's proficiency (van der Mass and Wagenmakers, 2005). In Figure 2d, respondents' ELO ratings are converted to a continuous red scale; as the lighter red scale, the lower ELO rating. For instance, a white dot indicates a respondent with a very low ELO rating. According to the figure, the respondents from the green group have higher ELO ratings, whereas those from the blue group have lower ELO scores. The red group appears to include those respondents with low and high ELO ratings, but those in the upper section have lower ELO ratings than those in the lower section, similar to the blue and green groups. This observation corresponds to the result of Figure 2c, which demonstrates the unobserved respondent's characteristic is well aligned in the interaction map.

Cumulative Incidence Functions (CIFs) We then examined CIFs for selected items and respondents from each cluster. Specifically, we chose one item from each cluster: Item 11 (blue), Item 28 (green), and Item 3 (red). We chose ten respondents from each cluster and marked them in hollow circles in Figures 2d and 2c. Figure 3 shows the CIFs for the selected items when the responses are correct (top row) and incorrect (bottom row). The CIFs for the ten selected respondents are drawn in each plot, where the line colors indicate their cluster membership. A respondent's CIF for correct and incorrect responses to the same item shows the opposite patterns as shown in Figure 3. Therefore, our analysis will be focused on the CIFs for correct responses to conserve space.

First, the peak height of CIF corresponds to the respondent's probability of giving a correct response. For example, respondents in blue have generally lower peaks than other respondents for Item 11, indicating that the blue group had a lower likelihood of getting Item 11 correct than other groups. Respondents in green show lower peaks in CIFs for Item 28 compared with two other items. This means that the group group had a lower likelihood of giving Item 28 correct compared with the other two items.

Second, how fast a CIF reaches its peak indicates how long it would take to give a correct response. For example, for Item 11, the CIFs of some respondents in the red group reach their peaks rapidly, while other respondents in the same red group reach their peaks much more slowly. This means that there was some degree of individual differences in the red group in terms of how long they would need to spend to give a correct response to Item 11. Recall that respondents and items were co-clustered when they are close in the interaction map, the CIFs tend to reach their peaks slowly when the respondents and items are in the same group (e.g., respondents in blue for Item 11).

Lastly, we found that $\Delta\hat{\theta}_k (> 1.5)$ are positive in the blue group, while $\Delta\hat{\theta}_k$ are negative and similar in the red and green groups. Note that despite the similarity in the global statistic $\Delta\hat{\theta}_k$, the red and green

groups are clearly differentiated in terms of the CIFs as shown in Figure 3. This suggests that examining CIFs provides additional insights for understanding the response processes of individual test-takers.

Model Fit: Posterior Predictive Checks We generate the posterior predictive samples of size 1,000 using Algorithm 1. The posterior predictive p-values (9), log-loss values (11), and AUCs are presented in Figure 4.

The posterior predictive p-values range between 0.05 and 0.95 for all items. AUCs range between 0.7 and 0.84 for most items. Log-loss values range between 0.2 and 0.6 for most items. We found that log-loss values are relatively large for difficult items. This may result from evenly distributed response times for the difficult items. Overall, these results suggest a reasonable fit of the proposed model for the ACT data.

4.2 App-based Language Assessment

4.2.1 Data and Estimation

The second data example is obtained from a mobile Language Learning App ‘Duolingo.’ The data were released for ‘The 2018 Duolingo Shared Task on Second Language Acquisition Modeling’¹. The data set includes responses to a set of test items given to individual app users. For analysis, we chose translation items, where users can translate a short sentence written in Spanish into English fully or by arranging given English words. For example, an item asks to translate a Spanish sentence ‘*Yo estoy bien.*’ into English: ‘*I am fine.*’, or to arrange three given words, “I”, “am”, and “fine”, into the correct order. Listening items were not included due to the large volume of missingness. There are two additional features to be discussed: (1) not all items are given to all test users. In other words, the number and kinds of items are different per user. For the sake of simplicity, we selected the users who responded to a common set of items; (2) there can be multiple responses to the same items given by the same users as the assessment system exposes identical items to users multiple times. We included the responses obtained at the first exposure if multiple responses appeared. As a result, 151 users responded to 18 items were included for data analysis.

This second data example from the app-based assessment is different from the ACT data set analyzed in the previous section in three ways: First, test items are similar to each other in terms of the format, structure, content, and difficulty levels. This means that items are less distinguishable among themselves than the items in the ACT data. Second, no time limit is set for each item or the entire test. This means

¹<http://sharedtask.duolingo.com/2018.html>

that users can spend on an item as long as they want, resulting in substantial variation in response times across items and respondents in this data set. Lastly, students' motivation levels are likely to vary to a large degree in this app-based, non-conventional kind of assessment. A lack of motivation may be responsible for large within- and between-person variations in response accuracy and times.

4.2.2 Analysis Results

Accumulation Rate Differences $\Delta\lambda_{i,j}$ Figure 5 summarizes the posterior distribution of $\Delta\lambda_{i,j}$. Response time was divided into five sub-intervals using the sample quantiles as cut-off points: 0 to 5 seconds for the first interval; 5 to 8 seconds for the second interval; 8 to 12 seconds for the third interval; 12 to 19 seconds for the fourth interval; and 19 to 200 seconds for the fifth interval. We considered that response time over 200 seconds were censored. Figure 5 shows that $\Delta\lambda_{i,j}$ are around 0 and rarely change across the time intervals for all items. This indicates that the accumulation rates between correct and incorrect responses are similar and generally do not change much over time. This is different from the ACT data analysis, where we observed meaningful differences in accumulation rate across the time intervals and test items.

Interaction Map The estimated interaction maps for the Duolingo data is presented in Figure 6a. As shown in Section 4.1.2, the interaction maps can differentiate subtle differences in the correctness of responses as well as the length of response times. For example, items 6, 8, 12, and 14 are located on the outskirts of the map, meaning that they are solved correctly by most users in a relatively short time compared with other items. In fact, these are the simplest items that only involve one or two words.

The spectral co-clustering is applied, and the result is shown in Figure 6b. Using the elbow method, we determine $K = 2$ is the optimal number of clusters in this dataset. The cluster membership is represented in red and blue colors.

In Figure 6c, we overlaid respondents with $\Delta\hat{\theta}_k$ using the same fashion in Section 4.1.2. The red cluster included near-zero or negative $\Delta\hat{\theta}_k$, implying that their accumulation rate was relatively higher when they gave a correct response. The blue cluster included respondents with positive $\Delta\hat{\theta}_k$ values, implying that their accumulation rates are relatively higher when they gave incorrect responses.

Lastly, we overlaid respondents with average response accuracy in Figure 6d. The respondents from the red group show generally higher response accuracy than the respondents in the blue group. This is consistent with our findings based on $\Delta\hat{\theta}_k$.

Cumulative Incidence Functions (CIFs) We then examined CIFs for selected items and respondents from each cluster. We chose one item from each cluster: Item 2 (blue) and Item 15 (red). We chose five respondents from each cluster and marked them in hollow circles in Figures 6c and 6d. Figure 7 shows the CIFs for the selected items when the responses are correct (top row) and incorrect (bottom row). The CIFs for the five selected respondents are drawn in each plot, where the line colors indicate their cluster membership. As in the ACT data, we focus on interpreting the CIFs for correct responses below.

In Figure 7, the blue CIFs tend to show lower peaks than the red CIFs. There are some individual differences among the respondents in reaching the peaks. For example, in the blue group, as the peak is high, the peaks are reached more slowly than when the peak is low. This means that to give a correct response, respondents would spend a longer time on solving items. For item 15, the peaks are generally lower than item 2 for respondents in both groups. The blue CIFs are similar for two items in terms of peaks and the time to reach the peaks. However, the red CIFs show quite different patterns for two items. The CIF of one respondent is peculiar and shows a different pattern than other respondents in the same group. Similar to the ACT data, these results suggest that examining CIFs offers valuable and additional insights into the response processes of individual test-takers.

Model Fit: Posterior Predictive Checks We evaluated the model fit for the Duolingo data based on 1,000 posterior predictive samples. Figure 8 shows posterior predictive p-values (9), log-loss values (11), and AUCs for the data.

The posterior predictive p-values appear less desirable than the ACT data example. This may be due to the large variation in the response times, which stems from no time limit given to this app-based assessment setting. We assumed response times above 200 seconds are censored. Thus, it may be more challenging to simulate response times close to the original data. The log-loss values and AUCs range between 0.25 and 0.75 and 0.5 and 0.75, respectively, and we concluded that the fit of the proposed model is acceptable for this dataset.

5 Conclusions

Connection times, how long it takes for a pair of nodes to be connected, have been under-studied in the social network literature. In the present study, we proposed a novel statistical modeling approach to study connection times between two types of nodes in a bipartite network. Motivated by a particular type of bipartite network composed of a group of test-takers and a set of test items from assessment

data, we aimed to examine how incorporating and modeling connection times in a bipartite network can shed new light on the nature and structure of the connections between two different types of nodes.

The significance of the present study can be summarized as follows: First, to our best knowledge, this is the first study in the literature to model connection times in a bipartite network. Second, our novelty also lies in that we modeled the dependence structures of connections and connection times within a competing risk modeling framework. This adoption was motivated by the need to address that the dependence structures of interest are likely to be heterogeneous between the two mutually exclusive outcomes of connection types, e.g., correct and incorrect responses in the context of assessment data. Such adaptation has not been utilized in the network literature. Third, we have demonstrated that the proposed approach can be a beneficial tool for studying connection types in a bipartite network composed of respondents and test items in the context of assessment data analysis. Our real data analysis showed that examining the estimated interaction map and cumulative incidence functions, as well as the posterior distribution of accumulation rate differences between the two connection types from our approach, offered unique and interesting insights on the process of connections for individual test-takers. Such information may be unobtainable with existing methods for response time analysis in the literature. Fourth, although our approach was motivated by a special type of bipartite network between respondents and test items, the proposed framework is general and can be applied to other types of bipartite networks where the two connection outcome types are believed to influence and shape the dependence structures of connections largely.

There can be many directions for extending the proposed framework for further generalization. For example, one interesting direction for future study is to extend the proposed approach to the settings where the types of connections are more than binary. Such an approach can be beneficial in assessment settings where multiple-choice items involve meaningful distractors. Often selecting different distractors rather than the correct option indicates different levels or types of cognitive functions. In this case, the extended framework will enable us to investigate how different distractors, i.e., connection outcome types, can shape the dependence structures of connection times between respondents and test items. This can show how individual test-takers interact differently with test items depending on their cognitive function types and levels. Such analysis can meaningfully improve our understanding of individual differences in the process of the cognitive functions of interest-based on connection times.

Acknowledgement

This study was partially supported by the Yonsei University Research Fund 2019-22-0210 and by Basic Science Research Program through the National Research Foundation of Korea (NRF 2020R1A2C1A01009881). Correspondence should be addressed to Ick Hoon Jin, Department of Applied Statistics, Department of Statistics and Data Science, Yonsei University, Seoul, Republic of Korea. E-Mail: ijin@yonsei.ac.kr.

References

Agneessens, F. and H. Roose (2008). Local structural properties and attribute characteristics in 2-mode networks: p^* models to map choices of theater events. *Journal of Mathematical Sociology* 32, 204–237.

Andersen, P. K., R. B. Geskus, T. de Witte, and H. Putter (2012). Competing risks in epidemiology: possibilities and pitfalls. *International journal of epidemiology* 41, 861–870.

Austin, P. C., D. S. Lee, and J. P. Fine (2016). Introduction to the analysis of survival data in the presence of competing risks. *Circulation* 133, 601–609.

Bomiriya, R. P. (2014). *Topics in Exponential Random Graph Modeling*. Ph. D. thesis, The Pennsylvania State University.

Brown, S. D. and A. Heathcote (2005). A ballistic model for choice response times. *Psychological Review* 112, 117–128.

Brown, S. D. and A. Heathcote (2008). The simplest complete model of choice response time: Linear ballistic accumulation. *Cognitive Psychology* 57, 153–178.

Carpenter, B., A. Gelman, M. D. Hoffman, D. Lee, B. Goodrich, M. Betancourt, M. Brubaker, J. Guo, P. Li, and A. Riddell (2017). Stan: A probabilistic programming language. *Journal of Statistical Software* 76.

Chakraborty, A., H. Krichene, H. Inoue, and Y. Fujiwara (2019). Exponential random graph models for the Japanese bipartite network of banks and firms. *Journal of Computational Social Science* 2, 3–13.

Cheng, S. C., L. J. Wei, and J. Ying (1995). Analysis of transformation models with censored data. *Biometrika* 82, 835–846.

Cheng, S. C., L. J. Wei, and J. Ying (1997). Predicting survival probabilities with semiparametric transformation models. *Journal of the American Statistical Association* 92, 227–235.

Cox, D. R. (1972). Regression models and life-tables (with discussion). *Journal of the Royal Statistical Society B* 34, 187–220.

Dhillon, I. S. (2001). Co-clustering documents and words using bipartite spectral graph partitioning. In *Proceedings of the seventh ACM SIGKDD international conference on Knowledge discovery and data mining*, New York, NY, USA, pp. 269–274.

Fine, J. P. and R. J. Gray (1999). A proportional hazards model for the subdistribution of a competing risk. *Journal of the American Statistical Association* 94, 496–509.

Fine, J. P., Z. Ying, and L. J. Wei (1998). On the linear transformation model with censored data. *Biometrika* 85, 980–986.

Friel, N., R. Rastelli, J. Wyse, and A. E. Raftery (2016). Interlocking directorates in Irish companies using a latent space model for bipartite networks. *Proceedings of the National Academy of Sciences of the United States of America* 113, 6629–6634.

Gelman, A. and D. B. Rubin (1992). Inference from iterative simulation using multiple sequences. *Statistical Science* 7, 457–472.

Gower, J. C. (1975). Generalized procrustes analysis. *Psychometrika* 40, 33–51.

Handcock, M. S., A. E. Raftery, and J. M. Tantrum (2007). Model-based clustering for social network. *Journal of the Royal Statistical Society, Series A* 170, 301–354.

Hoff, P., A. Raftery, and M. S. Handcock (2002). Latent space approaches to social network analysis. *Journal of the American Statistical Association* 97, 1090–1098.

Ibrahim, J. G., M.-H. Chen, and D. Sinha (2001). *Bayesian Survival Analysis*. New York: Springer.

Jeon, M., I. H. Jin, M. Schweinberger, and S. Baugh (2021). Mapping unobserved item–respondent interactions: A latent space item response model with interaction map. *Psychometrika* 86, 378–403.

Jin, I., S. Liu, P. Thall, and Y. Yuan (2014). Using data augmentation to facilitate conduct of phase I-II clinical trials with delayed outcome. *Journal of the American Statistical Association* 109, 525–536.

Kevork, S. and G. Kauermann (2022). Bipartite exponential random graph models with nodal random effects. *Social Networks* 70, 90–99.

Krivitsky, P. N., M. S. Handcock, A. E. Raftery, and P. D. Hoff (2009). Representing degree distributions, clustering, and homophily in social networks with latent cluster random network models. *Social Networks* 31, 204–213.

Larremore, D. B., A. Clauset, and A. Z. Jacobs (2014). Efficiently inferring community structure in bipartite networks. *Physical Review E* 90, 012805.

Latapy, M., C. Magnien, and N. Vecchio (2008). Basic notions for the analysis of large two-mode networks. *Social Networks* 30, 31–48.

Lau, B., S. R. Cole, and S. J. Gange (2009). Competing risk regression models for epidemiologic data. *American journal of epidemiology* 170, 244–256.

Lee, C. and D. J. Wilkinson (2019). A review of stochastic block models and extensions for graph clustering. *Applied Network Science* 4, 122.

Lusher, D., J. Koskinen, and G. Robins (Eds.) (2013). *Exponential Random Graph Models for Social Networks: Theory, Methods, and Applications*. New York, NY: Cambridge University Press.

Passino, F. S. and N. A. Heard (2020). Bayesian estimation of the latent dimension and communities in stochastic blockmodels. *Statistics and Computing* 30, 1291–1307.

R Core Team (2020). *R: A Language and Environment for Statistical Computing*. Vienna, Austria: R Foundation for Statistical Computing.

Raftery, A., X. Niu, P. Hoff, and K. Yeung (2012). Fast inference for the latent space network model using a case-control approximate likelihood. *Journal of Computational and Graphical Statistics* 21, 909–919.

Ranger, J. and J. Kuhn (2014). An accumulator model for responses and response time in tests based on the proportional hazards model. *British Journal of Mathematical and Statistical Psychology* 67, 388–407.

Robins, G. and M. Alexander (2004). Small worlds among interlocking directors: network structure and distance in bipartite graphs. *Computational & Mathematical Organization Theory* 10, 69–94.

Silk, M. J. and D. N. Fisher (2017). Understanding animal social structure: exponential random graph models in animal behaviour research. *Animal Behaviour* 132, 137–146.

Su, L., W. Lu, R. Song, and D. Huang (2020, April). Testing and Estimation of Social Network Dependence With Time to Event Data. *Journal of the American Statistical Association* 115(530), 570–582.

Sun, Y. (2021). *Bipartite Network Community Detection: Development and Survey of Algorithmic and Stochastic Block Model Based Methods*. Ph. D. thesis, University of California, Los Angeles.

Usher, M. and J. L. McClelland (2001). The time course of perceptual choice: The leaky, competing accumulator model. *Psychological Review* 108, 550–592.

van der Mass, H. L. J. and E.-J. Wagenmakers (2005). A psychometric analysis of chess expertise. *American Journal of Psychology* 118, 29–60.

Van Zandt, T., H. Colonius, and R. W. Proctor (2000). A comparison of two response time models applied to perceptual matching. *Psychonomic Bulletin & Review* 7, 208–256.

Vickers, D. (1970). Evidence for an accumulator model of psychophysical discrimination. *Ergonomics* 13, 37–58.

Walke, R. (2010, May). Example for a piecewise constant hazard data simulation in R. Technical Report TR-2010-003, Max Planck Institute for Demographic Research, Rostock.

Wang, P., P. Pattison, and G. Robins (2013). Exponential random graph model specifications for bipartite networks - a dependence hierarchy. *Social Networks* 35, 211–222.

Wang, P., G. L. Robins, P. Pattison, and E. Lazega (2013). Exponential random graph models for multilevel networks. *Social Networks* 35, 96–115.

Wang, P., K. Sharpe, G. L. Robins, and P. E. Pattison (2009). Exponential random graph (p^*) models for affiliation networks. *Social Networks* 31, 12–25.

Zhou, Z. and A. A. Amini (2019). Analysis of spectral clustering algorithms for community detection. *Journal of Machine Learning Research* 20, 1–47.

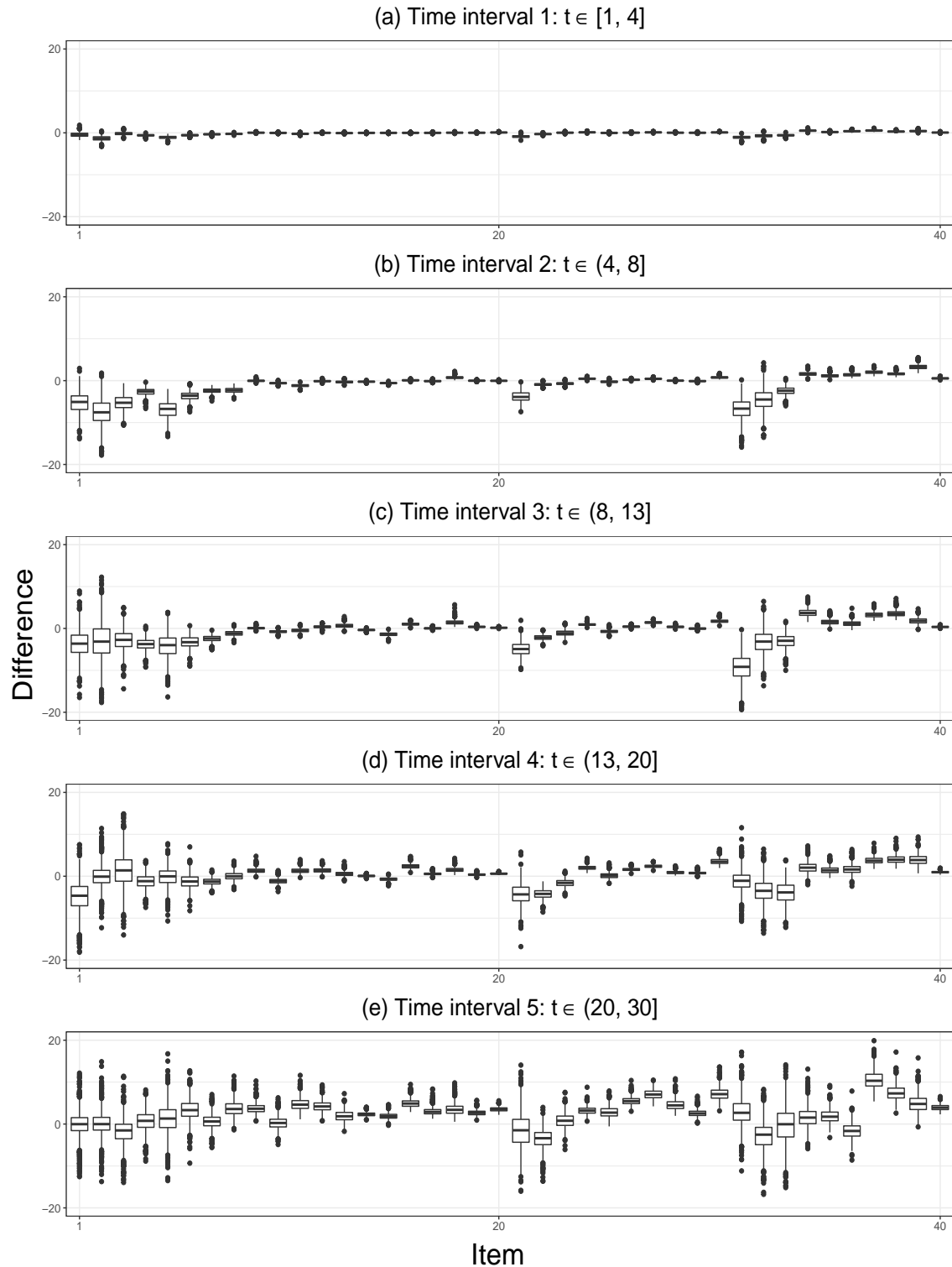
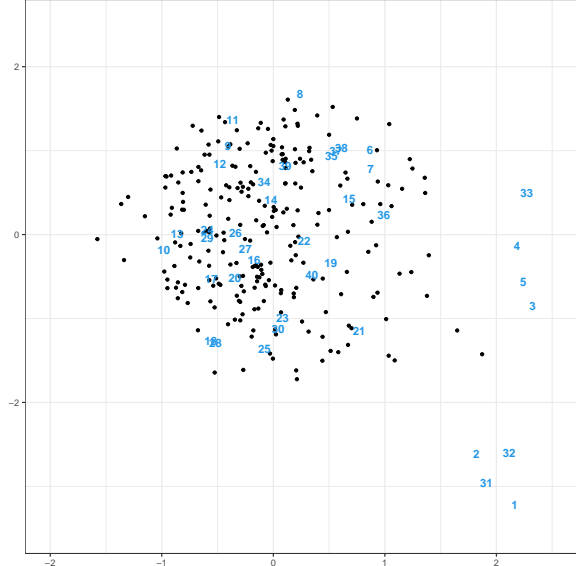
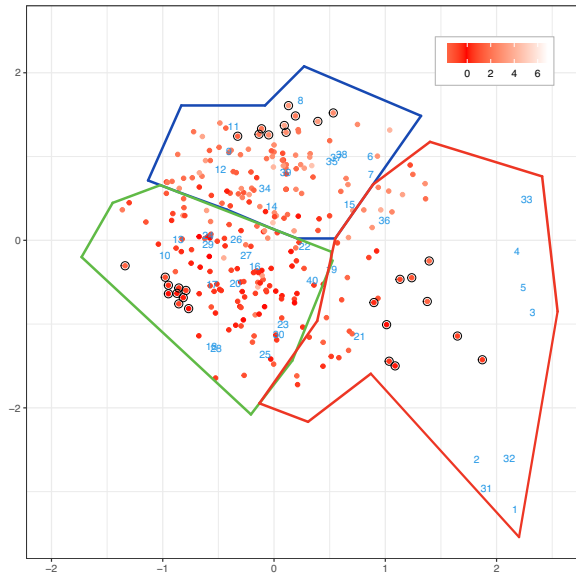


Figure 1: The posterior distribution of $\Delta\lambda_{i,j} = \lambda_{i(-1),j} - \lambda_{i(1),j}$. The response time t is divided into five time intervals ($j = 1, 2, \dots, 5$), and $\Delta\lambda_{i,j}$ for each item j are calculated for the time intervals.

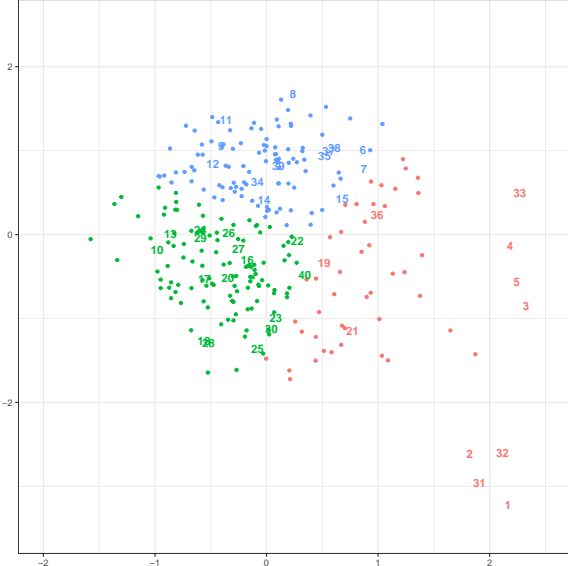
(a) Posterior means of latent embeddings. Dots represent respondents, and numbers represent Items.



(c) Posterior mean differences, $(\hat{\Delta}\theta_k = \hat{\theta}_{k(-1)} - \hat{\theta}_{k(1)})$ are converted to a red scale.



(b) Spectral co-clustering. Groups of items and respondents are marked using red, green, and blue.



(d) ELO ratings are converted to the red scale with white being the lowest and red being the highest.

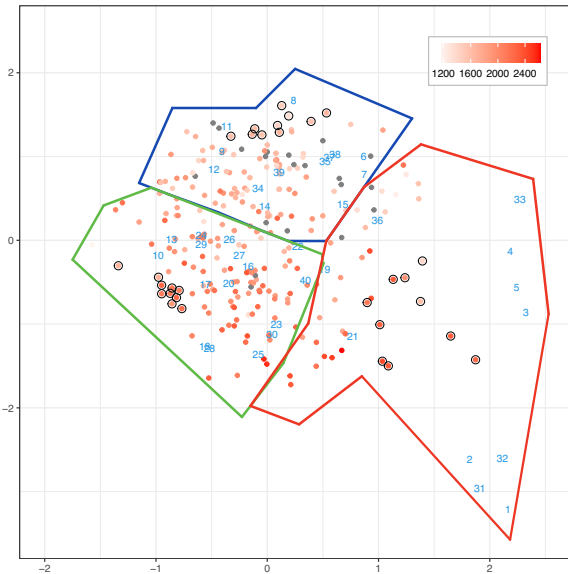


Figure 2: Interaction maps of latent embeddings estimated by the latent space accumulator model for ACT data.

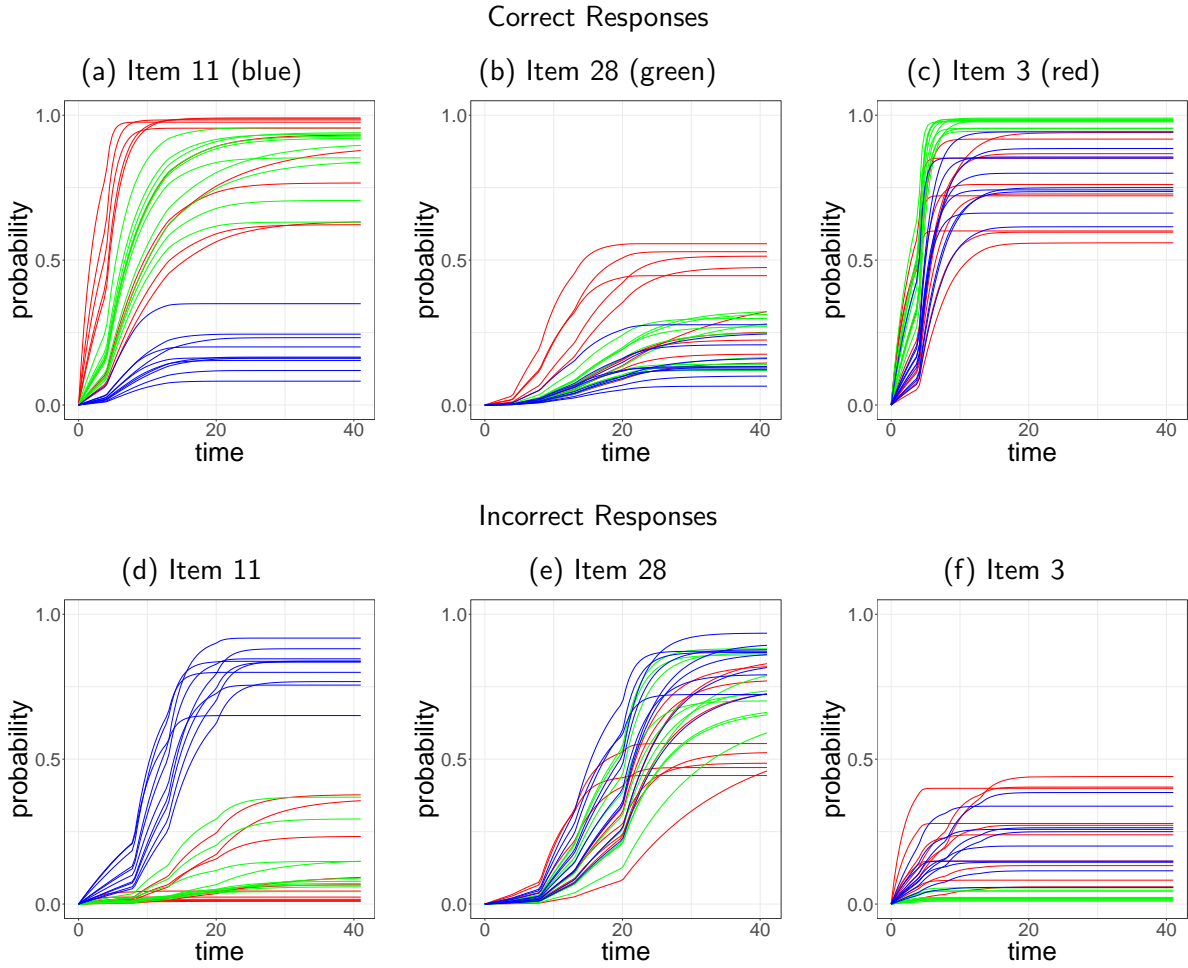


Figure 3: Cumulative incidence functions (CIFs) of selected respondents and items for ACT data. We select Item 11 from the blue cluster, Item 28 for the green, and Item 3 from the red. Each of the 10 respondents are chosen nearby their cluster centers, and marked by their cluster membership colors. We present correct response CIFs in the top panel, and incorrect response CIFs in the bottom.

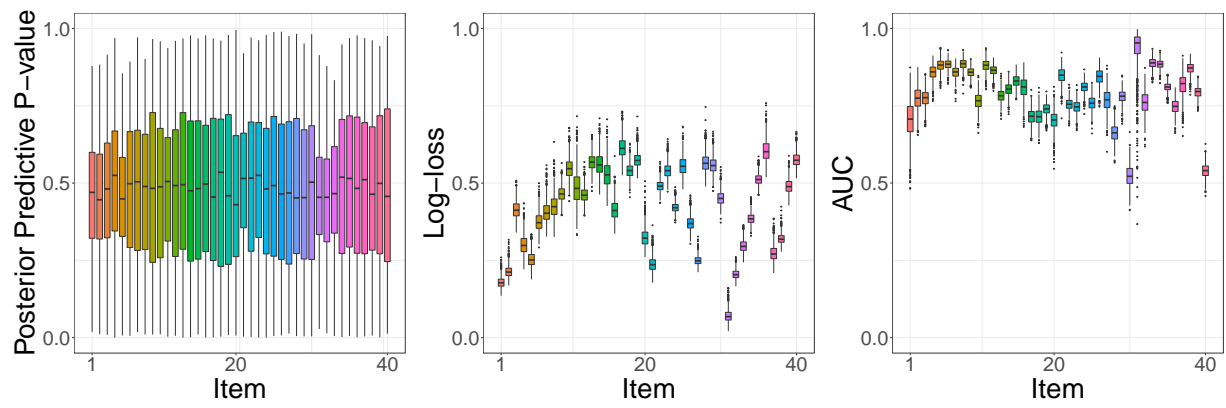


Figure 4: Model fit assessment for ACT data. Posterior predictive samples are generated to calculate posterior predictive p-values (left panel), the log-loss (middle panel), and AUC (right panel) for each item.

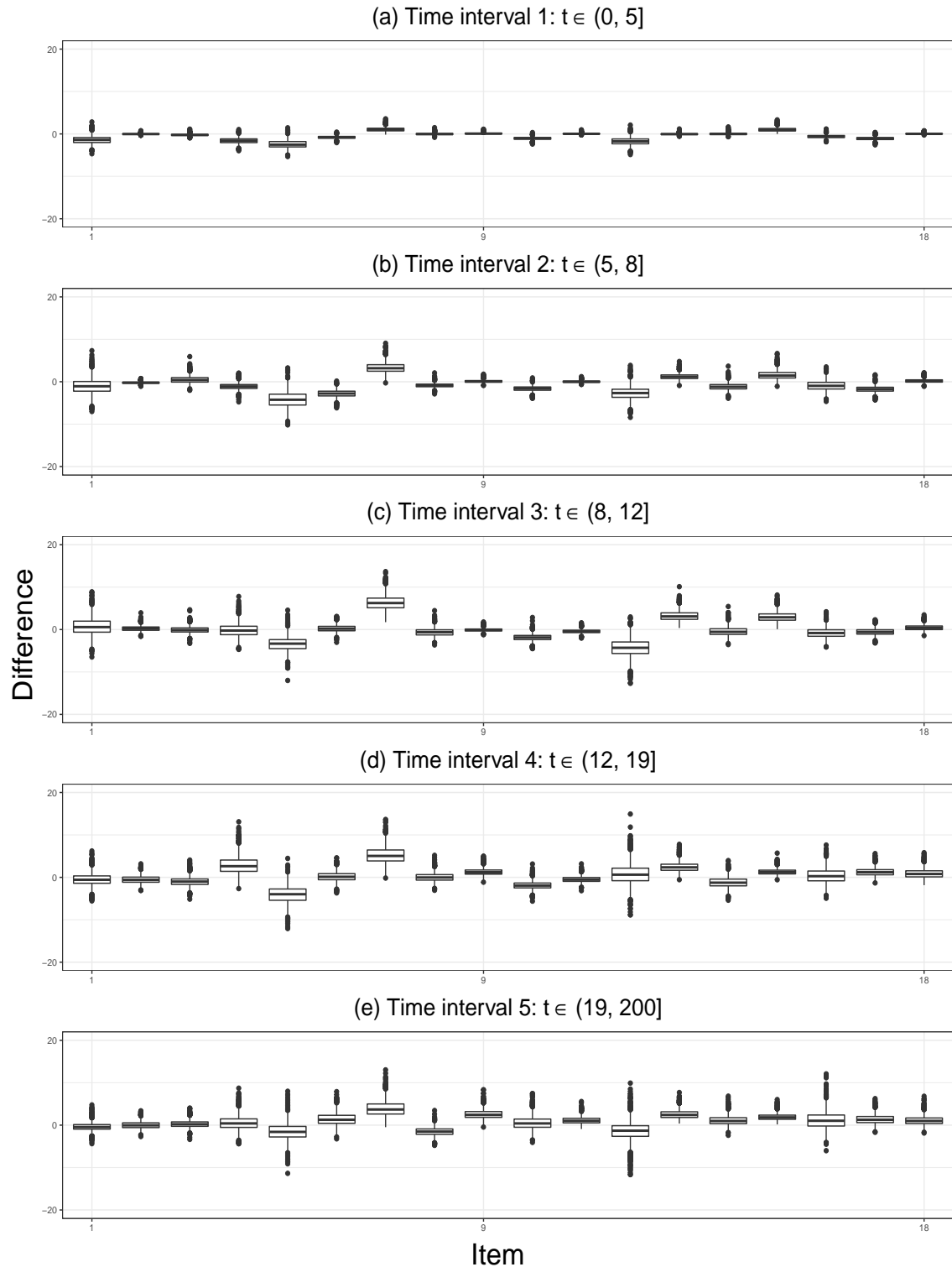
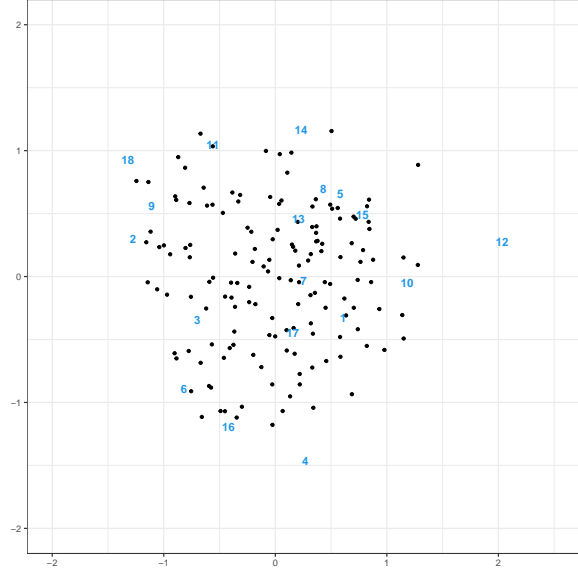
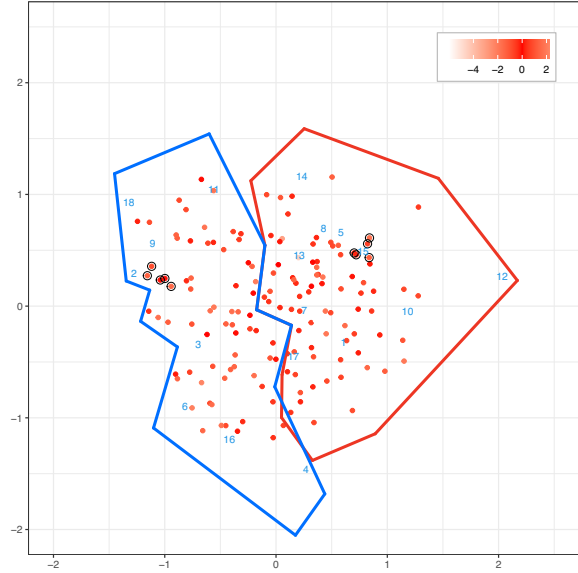


Figure 5: The posterior distribution of $\Delta\lambda_{i,j} = \lambda_{i(-1),j} - \lambda_{i(1),j}$. The response time t is divided into five time intervals ($j = 1, 2, \dots, 5$), and $\Delta\lambda_{i,j}$ for each item j are calculated for the time intervals.

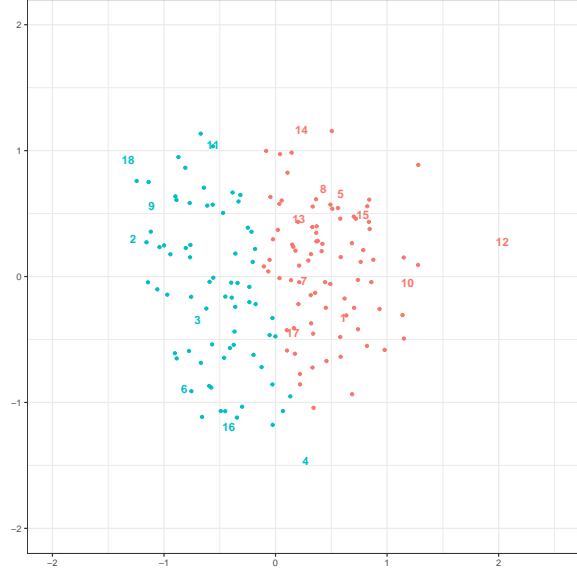
(a) Posterior means of latent embeddings. Dots represent respondents, and numbers represent items.



(c) Posterior mean differences, $(\hat{\Delta}\theta_k = \hat{\theta}_{k(-1)} - \hat{\theta}_{k(1)})$ are converted to a red scale.



(b) Spectral co-clustering. Groups of items and respondents are marked using red and blue.



(d) Accuracy rates are converted to the red scale with white being the lowest and red being the highest.

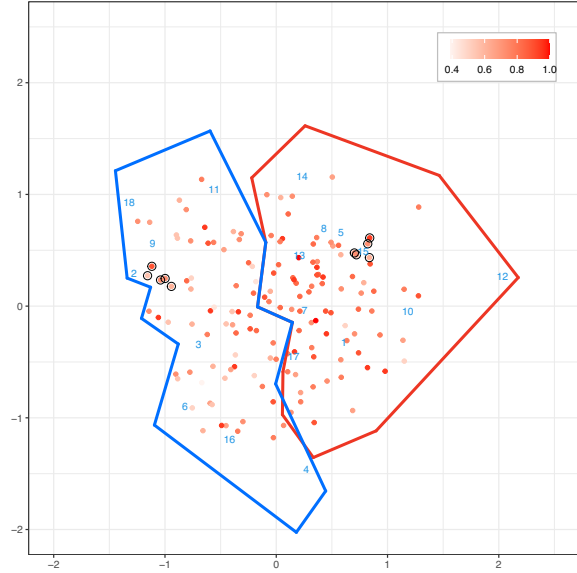


Figure 6: Interaction maps of latent embeddings estimated by the latent space accumulator model for Duolingo data.

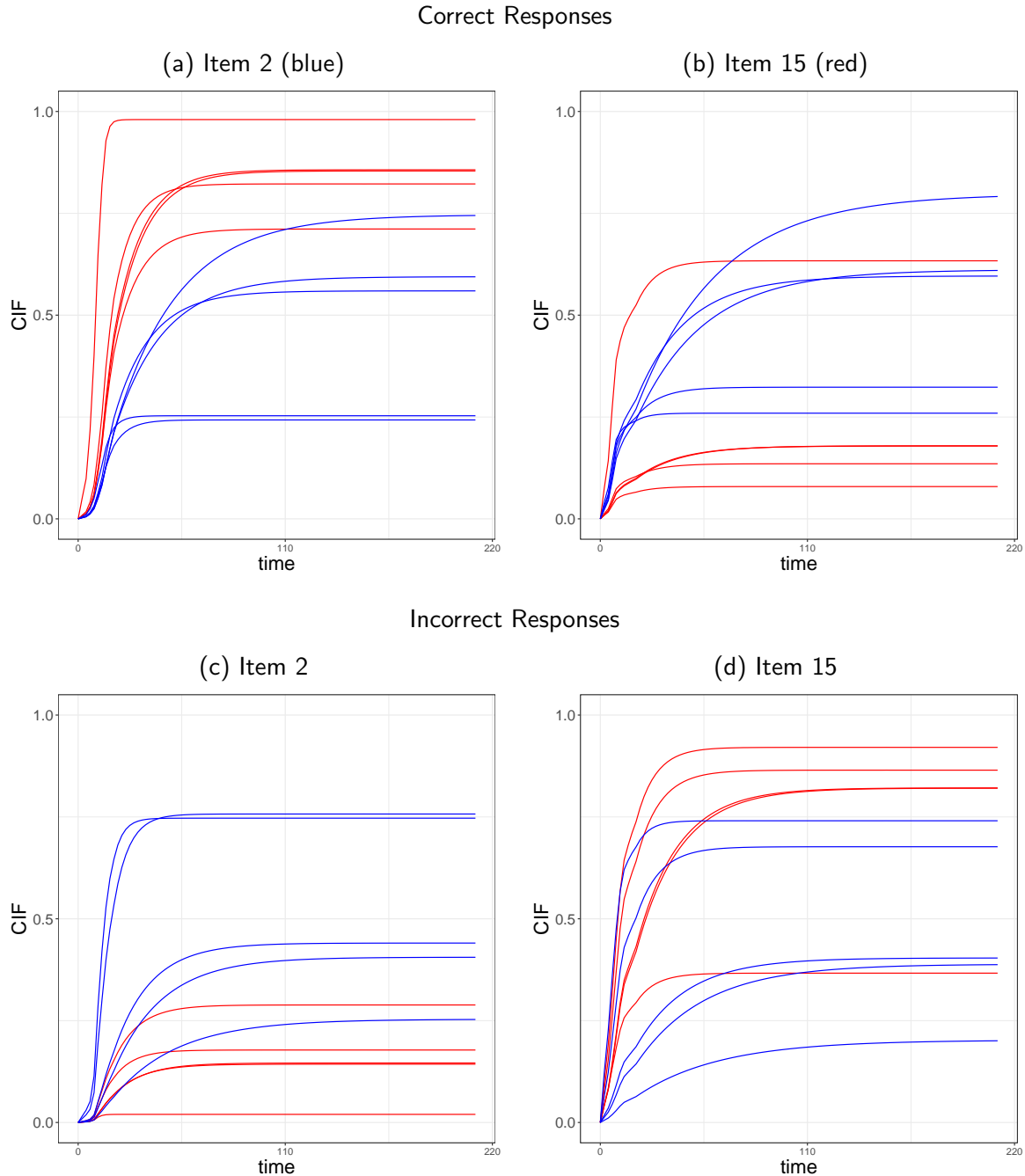


Figure 7: Cumulative incidence functions (CIFs) of selected respondents and items. We select Item 2 from the blue cluster and Item 15 from the red. Each of the 5 respondents are chosen nearby their cluster centers, and marked by their cluster membership colors. We present correct response CIFs in the top panel, and incorrect response CIFs in the bottom.

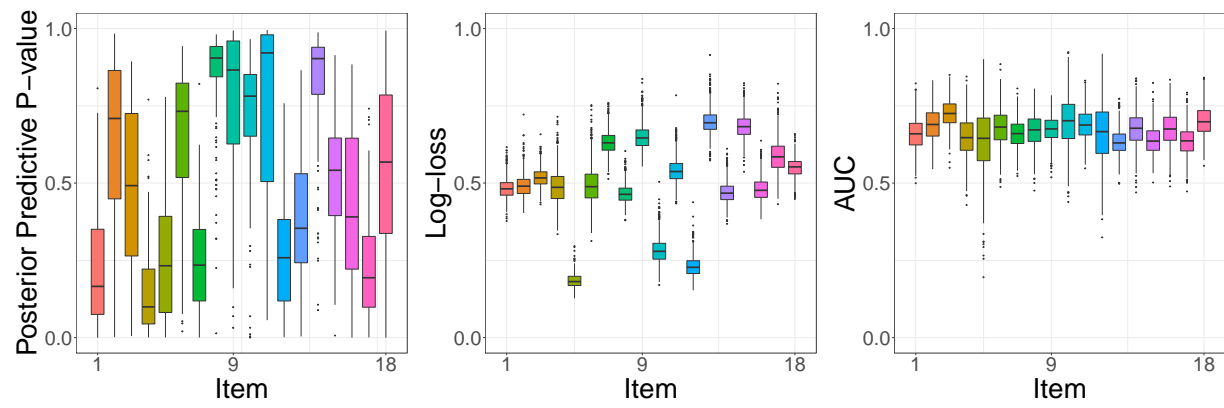


Figure 8: Model fit assessment for Duolingo data. Posterior predictive samples are generated to calculate posterior predictive p-values (left panel), the log-loss (middle panel), and AUC (right panel) for each item.